Jestr

Journal of Engineering Science and Technology Review 17 (2) (2024) 175 - 181

Research Article

JOURNAL OF
Engineering Science and Technology Review

www.jestr.org

Experimental Study on L-shaped Concrete-filled Steel Tubular Columns under Axial Compression and Eccentric Compression

Zhangqi Hu[1,2,*], Ran He[1], Jin Liu[1,3], Meng Wang[4] and Junyuan Zhang[1]

[1]*School of Civil Engineering, Hunan City University, Yiyang 413000, China*
[2]*Hunan Engineering Research Center of Development and Application of Ceramsite Concrete Technology，Hunan City University, Yiyang 413000, China*
[3]*Key Laboratory of Green Building and Intelligent Construction in Higher Educational Institutions of Hunan Province, Yiyang, 413000, China*
[4]*Hunan Zhongda Designing Institute Co., Ltd., Changsha, 411201, China*

Received 3 February 2024; Accepted 28 April 2024

Abstract

Special-shaped concrete-filled steel tubular columns are widely utilized in high-rise buildings. In order to further simplify the construction steps and increase the application scope, a novel L-shaped concrete-filled steel tubular column (LCFSTC) was proposed. Nine specimens, scaled at 1:1, were designed and grouped with specimen lengths of 0.5, 1.0, and 2.0 m. Compressive tests were performed on the nine specimens under various experimental parameters, including specimen length, concrete strength, and loading conditions (axial or eccentric loading). The tests aimed to verify the reliability of the LCFSTC and explore its mechanical properties by analysing failure modes, load-vertical deflection curves, load-rotation angle curves, and load-strain curves. Results demonstrate that no specimen experienced weld seam failure, indicating good structural integrity for the LCFSTCs. For the axial-loading specimens, the bearing capacity and ductility increase with the specimen length. As the specimen length increases from 0.5 m to 1.0 and 2.0 m, the ductility coefficient (mean value) decreases by 23.0% and 47.2%, respectively. Increasing the concrete strength can improve the bearing capacity; the average bearing capacity of the specimens with a concrete strength of C40 increases by 17.1% compared with that of the C30 specimens. Eccentric loading increases the lateral deformation and affects the strain distribution and bearing capacity. This study can provide a good reference for the application and design of special-shaped concrete-filled steel tubular columns.

Keywords: Special-shaped column, Axial compression test, Eccentric compression test, Concrete-filled steel tubular column, L-shaped column

1. Introduction

Special-shaped columns have been widely used in civil engineering [1, 2] It is typically desirable to enhance the mechanical performance of these columns while maintaining good applicability. Special-shaped concrete-filled steel tubular columns integrate the advantages of both concrete-filled steel tubular columns and reinforced concrete special-shaped columns. These column types not only increase the usable area and enhance aesthetic appeal but also offer good compressive performance and deformability [3, 4]. Thus, special-shaped concrete-filled steel tubular columns have experienced a growing trend in application and demand. Ease of construction, short construction periods, and building heights have also become common demands with advancements in the construction industry. Special-shaped concrete-filled steel tubular columns with optimized structural integrity and efficient construction techniques must be developed to ensure both safety and expedited construction processes.

Scholars have proposed a variety of special-shaped concrete-filled steel tubular columns and conducted investigations to improve their mechanical properties [5-7]. The most commonly used steel tubes in current research are rolled steel tubes. Although these special-shaped concrete-filled steel tubular columns possess high bearing capacity and good deformability, their section size and configuration are constrained by the dimensions of the rolled steel tubes. Welded steel tubes could offer greater flexibility in terms of section forms for special-shaped concrete-filled steel tubular columns compared to rolled steel tubes. Consequently, engineers can design special-shaped concrete-filled steel tubular columns more flexibly to align with architectural plans. Therefore, the utilization of welded steel tubes in constructing special-shaped concrete-filled steel tubular columns can streamline construction and broaden their application. In this context, this study proposes a novel L-shaped concrete-filled steel tubular column (LCFSTC) constructed by welding two square steel tubes and one angle steel, aiming to further simplify the construction steps and expand the application scope. However, this research topic has received relatively less attention, indicating the need to further validate reliability parameters.

Thus, nine specimens were designed and subjected to compression tests in this study to verify the reliability of the novel L-shaped concrete-filled steel tubular column and to explore its mechanical properties. This study investigated the effects of specimen length, concrete strength, and loading conditions (axial or eccentric loading) on the mechanical properties of LCFSTCs. The findings of this research could offer valuable insights for the application and design of concrete-filled steel tubular columns.

*E-mail address: huzhangqi0413@163.com
ISSN: 1791-2377
doi:10.25103/jestr.172.18

2. State of the art

Scholars have conducted extensive research on the mechanical properties of special-shaped concrete-filled steel tubular columns [2-18]. Alatshan et al. [2] conducted a comprehensive review summarizing the research on concrete-filled steel tubular columns, including tests on static axial compression, pure bending, combined static loading actions, etc. Krishan et al. [3] proposed a calculation method for short concrete-filled steel tube columns under compression. The comparison between the theoretical and experimental results indicated that the developed calculation procedure can provide a reliable estimate of the stress-strain state and predict the load capacity of concrete-filled steel tube columns. Ahmed et al. [4] conducted compression tests on twenty square concrete-filled double steel tubular short columns, with sixteen subjected to eccentric loading, and four subjected to concentric loading. The results indicated that increasing eccentricity significantly reduces both the ultimate loads and the initial bending stiffness of square concrete-filled double steel tubular short columns. Zhang et al. [5] conducted axial compression tests on seven L-shaped concrete-filled steel tubular columns, each consisting of double vertical steel plates. On the basis of the test results, finite element analysis was performed to investigate the influence of specimen length and steel plate thickness on the axial compression performance of these L-shaped concrete-filled steel tubular columns. The test results and finite element analysis resulted in the development of a calculation method for the axial compression capacity, which exhibited good agreement with the finite element analysis results. Giakoumelis et al. [6] conducted a study on circular concrete-filled steel tubes (CFT) to investigate the influence of concrete strength on the bond strength between the concrete and the steel tube. The test results indicated that the bond of the concrete and the steel tube increases along with the concrete strength. Rozylo [7] presented experimental tests and numerical analyses to investigate the stability and failure analysis of thin-walled composite columns with a top-hat and channel cross-section. The results showed that the composite columns with a top-hat cross-section exhibited a higher load capacity than those with a channel cross-section. Bahrami et al. [8] conducted a study on the compression behavior of stiffened concrete-filled steel composite (CFSC) stub columns through finite element analysis, an equation was subsequently proposed to predict the loading capacity of CFSCs. The proposed equation was demonstrated to accurately predict the loading capacity of CFSCs. Tokgoz and Dundar [10] conducted an investigation into the impact of steel fibers on the behavior of L-shaped high-strength reinforced concrete and concrete-encased composite columns. The study involved testing sixteen specimens. The findings indicated that the addition of steel fibers to high-strength concrete significantly affects the structural behavior of both reinforced concrete and composite columns under biaxial bending and axial load. Chen et al. [11] designed 22 specimens to study the normal section bearing capacity of steel-reinforced concrete (SRC) special-shaped columns. Among these, 14 specimens underwent static loading tests, and 8 were subjected to low-cycle reversed loading tests. Subsequently, finite element analysis was conducted to investigate the influences of the loading angle, steel disposition form, sectional steel ratio, concrete strength grade, and depth-thickness ratio of the column limb on the normal section bearing capacity of SRC special-shaped columns. The research results indicate that the normal section bearing capacity of SRC special-shaped columns can be effectively improved by increasing the sectional steel ratio, concrete strength, and depth-thickness ratio. Yan et al. [12] introduced a unified algorithm for the eccentric-loaded capacity of special-shaped concrete-filled steel tubular columns by analyzing calculation methods in typical specifications. Their algorithm could help enhance computational theories for these columns. Liu et al. [13] proposed a novel type of L-shaped steel tubular concrete column. They conducted axial compression tests and eccentric compression tests on four full-scale specimens, followed by finite element analysis, and all the specimens exhibited an overall stable failure mode. Additionally, the bearing capacity of the specimens under eccentric compression was influenced by the eccentricity direction, column height, steel tube thickness, and concrete strength. Wang et al. [14] proposed a new special-shaped composite column (SS-CFSST) comprising multiple square steel tubes connected by steel hoops and conducted axial compression tests on eight specimens to investigate the impact of section shape, construction method, slenderness ratio, steel tube thickness, and steel strength on the compression performance of SS-CFSSTs. The study revealed that the hoop-type specimen has a greater loading capacity than the weld-type specimen. Aiming to investigate the ductility of rectangular composite concrete-filled steel tube (CFST) columns under axial compression, Grzeszykowski et al. [15] performed a test on 21 CFST columns and 5 steel columns. The test results indicated that the ductility of CFST columns highly depends on their failure mode, with the energy dissipation ability greatly influencing ductility. Ma et al. [16] performed an eccentric compression test on seven specimens to explore the feasibility of applying recycled aggregate concrete in L-shaped columns composed of concrete-filled steel tubes (RACFSTs). The results indicated that the strength of concrete decreased with increasing recycled aggregate replacement ratio, and the presence of steel tubes mitigated the influence of the recycled aggregate replacement ratio on the bearing capacity. Increasing the eccentricity decreased the bearing capacity of the RACFSTs. Hu et al. [17] performed finite element analysis and investigated the bearing capacities of multicell special-shaped concrete-filled steel tubular (MS-CFST) columns under axial loading, bending moments, and eccentric loading. On the basis of the analysis results, a unified calculation method was proposed to predict the performances of the four common combination forms of MT-CFST sections subjected to axial, eccentric, and pure bending loads, and the calculation results were in good agreement with the finite element analysis results. Yang et al. [18] conducted axial compression tests and eccentric compression tests on a batch of T-shaped concrete-filled steel tubular columns to investigate the effects of tensile bar stiffeners, specimen length, and eccentricity on the compressive performance of these columns. The test results indicated that the tensile bar stiffeners effectively delayed local buckling, and the steel tube stiffened by the tensile bars provided greater confinement for the concrete, thereby improving the concrete failure mode and increasing the concrete compressive strength of the T-shaped steel tube and enhancing the buckling resistance.

Previous studies have investigated the mechanical properties of special-shaped concrete-filled steel tubular columns with various cross-sections that commonly use rolled steel tubes. These steel tubes possess good mechanical properties, and their section size and form are restricted by the dimensions of the rolled steel tubes. The utilization of welded steel tubes can provide designers with the flexibility to customize the sections of special-shaped concrete-filled steel

tubular columns according to architectural blueprints. Therefore, employing welded steel tubes for constructing special-shaped concrete-filled steel tubular columns helps to simplify construction processes and enhance their versatility. The special-shaped concrete-filled steel tubular columns transition into an eccentric stress state postyielding, which impacts the stress distribution of the column and directly influences its failure mode, load-bearing capacity, and ductility. The specimen length, concrete strength, and eccentricity of specimens play pivotal roles in determining the stress distribution of special-shaped columns [5-8, 16]. However, concrete-filled steel tubular columns constructed with welded steel tubes are rarely discussed in current research. Further investigation is required to verify and explore the mechanical properties of these columns with varying specimen lengths, concrete strengths, and loading conditions.

In response to the limitations of existing research, this study proposes a novel LCFSTC. Nine specimens were divided into three groups for designing the specimen length and tested under compression to explore the mechanical properties of the LCFSTCs. The experimental parameters included specimen length, concrete strength, and loading conditions (axial or eccentric loading). This study can provide a reference for the application and design of special-shaped concrete-filled steel tubular columns.

The remainder of this study is organized as follows: Section III introduces the test design and loading device. Section IV presents the test results, discusses the failure modes of each specimen and explores the effects of specimen length, concrete strength, and loading conditions on the mechanical properties of LCFSTCs by analyzing load-vertical deflection curves and load–strain curves. Section V summarizes the study and draws conclusions.

3. Methodology

3.1 Test design

In this test, nine L-shaped concrete-filled steel tubular columns were grouped according to specimen length, with each group featuring specimen lengths of 0.5m, 1.0m, and 2.0m, all at a reduced scale of 1:1. The experimental parameters included specimen length, concrete strength, and loading conditions. The square steel tubes used in the test were welded steel tubes measuring 100 mm × 100 mm × 4 mm, and the L100 mm × 6 mm angle steel was used. An L-shaped steel tube was formed by welding two square steel tubes and one angle steel tube. Subsequently, a 30 mm-thick steel plate was welded beneath the L-shaped steel tube. The concrete was then poured into the L-shaped steel tube, followed by the welding of another 30 mm-thick steel plate on top after the concrete had cured. Fig. 1 illustrates the section dimensions, and the specific design parameters of each specimen are detailed in Table 1.

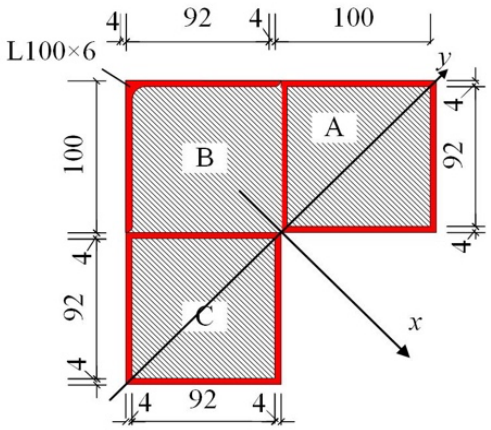

Fig. 1. Sectional dimensions (mm)

The steel grade used in the test is Q235, the average compressive strengths of the concrete (f_{cu}) for strength grades C30 and C40 were 32.7 and 43.2 MPa, respectively. The average strengths were determined by testing three cubic specimens, each measuring 150 mm × 150 mm × 150 mm. The material properties of the steel are detailed in Table 2.

Table 1. Design parameters of each specimen

Specimen No.	Specimen length *L* (m)	Concrete strength grade	Loading conditions (eccentricity)
LCC0.5-30-A	0.5	C30	Axial loading (0 mm)
LCC0.5-40-A	0.5	C40	Axial loading (0 mm)
LCC0.5-30-E	0.5	C30	Eccentric loading (20 mm)
LCC1.0-30-A	1.0	C30	Axial loading (0 mm)
LCC1.0-40-A	1.0	C40	Axial loading (0 mm)
LCC1.0-30-E	1.0	C30	Eccentric loading (20 mm)
LCC2.0-30-A	2.0	C30	Axial loading (0 mm)
LCC2.0-40-A	2.0	C40	Axial loading (0 mm)
LCC2.0-30-E	2.0	C30	Eccentric loading (20 mm)

Table 2. Mechanical properties of the steel

Type	Yield strength f_y (MPa)	Ultimate strength f_u (MPa)	Elastic modulus E_s(MPa)	Yield strain $\varepsilon_y(10^{-6})$
Square steel tube	268	410	2.06×10^5	1300.9
angle steel	373	432	2.06×10^5	1810.6

3.2 Test setup and measuring scheme

The centroid position and loading point of each specimen were calculated initially, followed by the installation of two hinge supports on the top and bottom steel plates. A 5000 kN hydraulic press was used to apply a compressive load, and four displacement meters were arranged at the four corners beneath the top steel plate to measure the vertical displacement. The 0.5 and 1.0 m-long specimens were equipped with six horizontal displacement meters, three of which were allocated to each zone (A and C), to record the lateral deflections. For the 2.0 m-long specimens, five horizontal displacement meters were installed in zones A and C, respectively. A, B, and C represent the three zones, while E, S, W, and N denote the four directions of east, south, west, and north, respectively. V represents the vertical strain gauge, and H represents the horizontal strain gauge. For the 1.0- and 2.0-m-long specimens, three rows of strain gauges were

installed, each containing 8 horizontal and 8 vertical strain gauges. These rows were positioned at one-fourth, one-half, and three-fourths of the specimen length. The 0.5 m-long specimens were equipped with strain gauges only at the midpoint of their length. The displacements and strains were recorded during the test. For safety, protective guards were placed around, and protective belts were installed during the tests. The protective belts remained unstressed during the loading process. Force control was applied incrementally, with each step increasing by 100 kN before reaching the maximum load. After reaching the maximum load, displacement control was used for incremental loading until specimen failure. Each load was sustained for 3~5 minutes to observe the test phenomena. The arrangement of strain gauges and horizontal displacement is shown in Fig. 2. And Fig.3 shows the test setup.

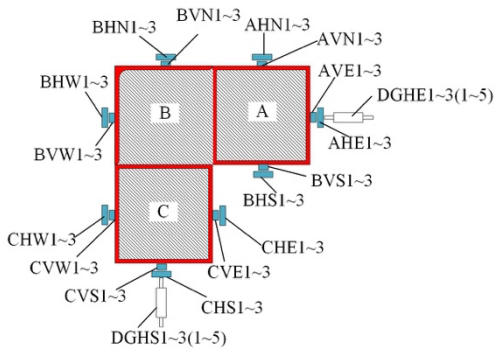

Fig. 2. Arrangement of strain gauges and horizontal displacement

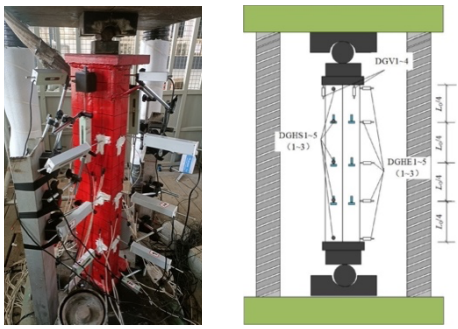

(a) (b)

Fig. 3. Test setup

4. Result Analysis and Discussion

4.1 Test phenomenon and failure modes

Fig. 4 shows the failure modes of nine specimens, none of which exhibited weld damage, indicating good synergistic performance among the square steel tubes and angle steel.

Specimens LCC0.5-30-A and LCC0.5-40-A showed no obvious signs of deformation up to 80% N_m (where N_m denotes the maximum load), indicating an elastic state. However, upon reaching 90% N_m, a slight bulge appeared in the steel tubes. Subsequently, both specimens exhibited slight bending deformation around the y-axis, accompanied by a slight abnormal sound. The load started to decrease as it approached the maximum, while the bending deformation gradually increased, eventually leading to failure due to excessive drum deformation. Both specimens exhibited multi-sided bulging deformation along their length, demonstrating clear characteristics of strength failure.

Specimen LCC0.5-30-E exhibited noticeable bending deformation at a 50% N_m loading step. Upon reaching 85% N_m, a slight bulge appeared on the steel tube surface, accompanied by an unusual sound. As the loading continued, the bending deformation increased rapidly. At the 2000 kN loading step, the specimen reached its maximum load, showing bulging on multiple sides accompanied by pronounced bending deformation. Specimen LCC0.5-30-E exhibited not only a strength failure mode but also a bending instability failure mode.

Specimens LCC1.0-30-A, LCC1.0-40-A, LCC1.0-30-E, LCC2.0-30-A, LCC2.0-40-A, and LCC2.0-30-E exhibited similar failure modes, characterized by severe bending deformation leading to failure due to local buckling instability. In the case of LCC1.0-30-A and LCC1.0-40-A, visible bending deformation occurred almost simultaneously with bulging. Conversely, for specimens LCC1.0-30-E, LCC2.0-30-A, LCC2.0-40-A, and LCC2.0-30-E, visible bending deformation was observed before bulging.

The shorter the specimen is (i.e., the smaller the slenderness ratio is), the more pronounced the observed bulging, and the bulging load of the axial-loaded specimens decreases with increasing specimen length. As the specimen length increased from 0.5 m to 1.0 and 2.0 m, the bulging load (average value) decreased by 11.9% and 16.7%, respectively. For the eccentric-loading specimens, the specimen length has a negligible impact on the bulging load, which is concentrated in the range of 1600 to 1700 kN. Eccentric-loading specimens and those with a large slenderness ratio exhibited obvious bending deformation, with bulging loads slightly lower than those of the axial-loading specimens and those with a small slenderness ratio.

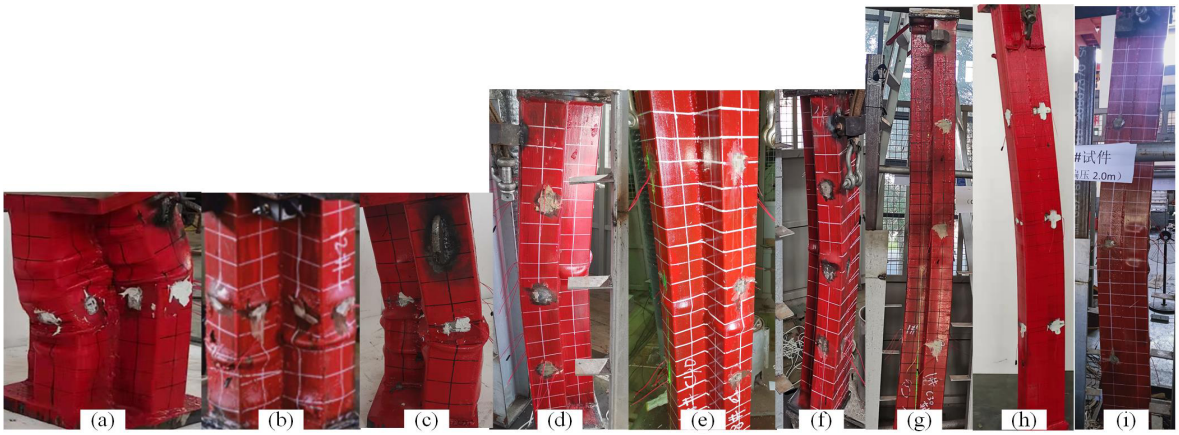

(a) LCC0.5-30-A; (b) LCC0.5-40-A; (c) LCC0.5-30-E; (d) LCC1.0-30-A; (e) LCC1.0-40-A; (f) LCC1.0-30-E; (g) LCC2.0-30-A; (h) LCC2.0-40-A; (i) LCC1.0-30-E

Fig. 4. Failure modes of the specimen

4.2 Load-vertical deflection curves

Fig. 5 shows the load−vertical deflection curves of the specimens, revealing an almost linear relationship between the vertical deflection and load before bulging. Eccentric loading accelerates the onset of bulging, but it does not significantly affect the vertical deformation performance of the 0.5 m-long specimens. The specimen length (slenderness ratio) greatly influences the ductility and bearing capacity of LCFSTCs. Both the ductility coefficient and bearing capacity of the axial-loaded specimens decrease as the specimen length increases. As the specimen length increased from 0.5 m to 1.0 and 2.0 m, the bearing capacity (mean value of specimens with C30 and C40 concrete grates) decreased by 2.5% and 11.1%, respectively, and the ductility coefficient decreased by 23.0% and 47.2%, respectively. In the case of eccentric-loaded specimens, especially those with a large slenderness ratio, significant bending deflection was observed. This phenomenon led to the angle steel (zone B) of specimen LCC2.0-30-E yielding under tension and subsequently entering the strengthening phase. This situation delays the occurrence of the maximum load but results in a higher bearing capacity than that of specimens LCC2.0-30-A and LCC1.0-30-E. The bearing capacity of LCFSTCs increases with increasing concrete strength. The average bearing capacity increases by 17.1% when the concrete strength increases from C30 to C40. Table 3 summarizes the characteristic load and deflection of the specimens, in which the yield deflection is calculated according to the method shown in Fig. 6.

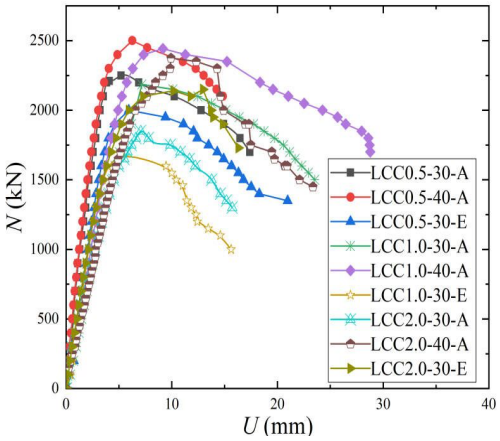

Fig. 5. Load–vertical deflection curves

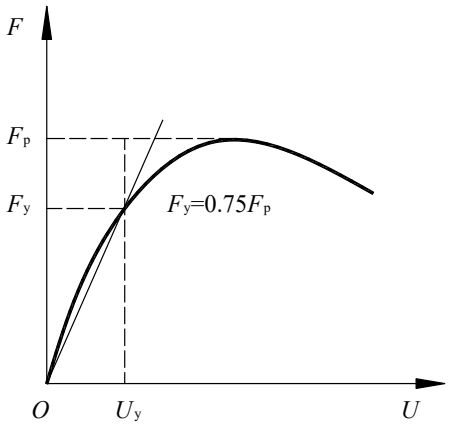

Fig. 6. Calculation method for yield deflection

Table 3. Characteristic load and deflection of the specimens

Specimen No.	U_b (mm)	N_b (kN)	U_y (mm)	N_y (kN)	U_m (mm)	N_m (kN)	U_u (mm)	N_b / N_m	μ
LCC0.5-30-A	3.22	2000	2.54	1687.5	5.20	2250	14.63	0.89	5.75
LCC0.5-40-A	4.05	2200	2.76	1875.0	6.27	2500	14.55	0.88	5.27
LCC0.5-30-E	3.65	1700	3.09	1500.0	5.94	2000	14.31	0.85	4.63
LCC1.0-30-A	6.21	1900	4.80	1639.5	7.18	2186	18.58	0.87	3.87
LCC1.0-40-A	4.30	1800	4.40	1832.3	9.17	2443	20.33	0.74	4.62
LCC1.0-30-E	3.73	1600	2.73	1275.0	5.31	1700	11.09	0.88	4.06
LCC2.0-30-A	6.61	1800	4.05	1387.5	7.06	1850	12.65	0.97	3.12
LCC2.0-40-A	5.15	1700	5.50	1781.3	9.92	2375	14.85	0.72	2.70
LCC2.0-30-E	3.84	1600	3.89	1612.5	12.03	2150	15.46	0.74	3.97

Note: N_b and U_b denote the bulging load and bulging deflection, respectively; N_y and U_y represent the yield load and the yield deflection, respectively; N_m is the maximum load; U_m is the maximum vertical deflection; U_u is the ultimate vertical deflection, which is the corresponding deflection when the load drops to $85\%N_m$; and μ is the ductility coefficient, which can be calculated as $\mu=U_u / U_y$.

4.3 Load-rotation angle curves

Fig. 7 illustrates the calculation method for the rotation angle (θ), which reflects the bending deformation of special-shaped columns. As the specimens bend around the y-axis, the rotation angle for 0.5 and 1.0 m-long specimens can be calculated by Eq. (1), while for the 2.0 m-long specimens, θ can be calculated by Eq. (2).

$$\theta = \frac{\sqrt{(\Delta_{E2} - \Delta_{E1})^2 + (\Delta_{S2} - \Delta_{S1})^2}}{L_0 / 2} \quad (1)$$

$$\theta = \frac{\sqrt{(\Delta_{E3} - \Delta_{E1})^2 + (\Delta_{S3} - \Delta_{S1})^2}}{L_0 / 2} \quad (2)$$

where L_0 is the distance between the top and bottom horizontal displacement meters. For the 0.5, 1.0, and 2.0 m-long specimens, L_0 is 0.4, 0.9, and 1.9 m, respectively; Δ_{E1}, Δ_{E2}, and Δ_{E3} represent the eastward horizontal deflections, which are measured by the bottom displacement sensors of all specimens, the middle displacement sensors of the 0.5 and 1.0 m-long specimens, and the middle displacement sensors of the 2.0 m-long specimens, respectively. Similarly, Δ_{S1}, Δ_{S2}, and Δ_{S3} are the southward horizontal deflections, which are measured by the bottom displacement sensors of all specimens, middle displacement sensors of 0.5 and 1.0 m-long specimens, and middle displacement sensors of 2.0 m-long specimens, respectively.

Fig. 8 shows the load–rotation angle curves. It can be illustrated that, the rotation angle of each specimen is nearly linear with the load during the early loading steps. After yielding, the lateral deflection increased significantly, and this increase was especially pronounced for the eccentric-loaded

specimens, indicating that they were greatly affected by the second-order effect of gravity and hence experienced severe bending deformation. The rotation angles of specimens LCC0.5-30-E, LCC1.0-30-E, and LCC2.0-30-E are 4.28, 1.99, and 7.16 rad, respectively.

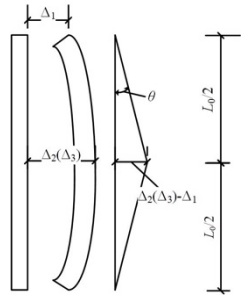

Fig. 7. Calculation method for the rotation angle

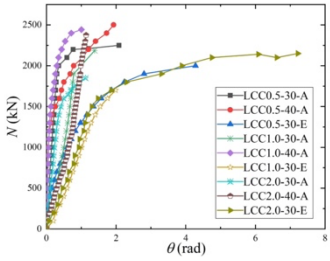

Fig. 8. Load–rotation angle curves

4.4 Load-strain curves

Fig. 9 presents the load–strain curves (N–ε curves) for the vertical strain in zones A, B, and C, measured at the midpoint of their lengths. Before yielding, the strains of the square steel tubes (zones A and C) and angle steel (zone B) increased almost simultaneously. After yielding, the strain of the angle steel increased slowly and even exhibited negative growth. In the case of eccentric-loaded specimens, the angle steel yielded in tension, while the square steel tubes reached the yield strain before the specimens yielded. This phenomenon is primarily attributed to eccentric loading enhancing the uneven force distribution, causing zones A, B, and C to experience nonuniform forces. In this scenario, compression loads are primarily borne by zones A and C, resulting in relatively minor compressive strain in the angle steel of zone B. Given that eccentric loading accentuated the second-order effect of gravity, specimens LCC0.5-30-E, LCC1.0-30-E, and LCC2.0-30-E exhibited significant bending deformation. The angle steel underwent a transition from compression to tension, and all eccentric-loaded specimens exhibited tensile yielding in the angle steel. The larger the slenderness ratio is, the greater the tensile strain in the later loading steps of the angle steel, indicating an increased prominence of the second-order effect of gravity with an increase in the slenderness ratio. The tensile strains of the angle steel for specimens LCC0.5-30-E, LCC1.0-30-E and LCC2.0-30-E reached 2024$\mu\varepsilon$, 2936$\mu\varepsilon$, and 7150 $\mu\varepsilon$, respectively. Before yielding, specimens with a concrete strength grade of C40 exhibited lower compressive strain in the square steel tubes than that of the axial-loaded specimens with a concrete strength grade of C30.

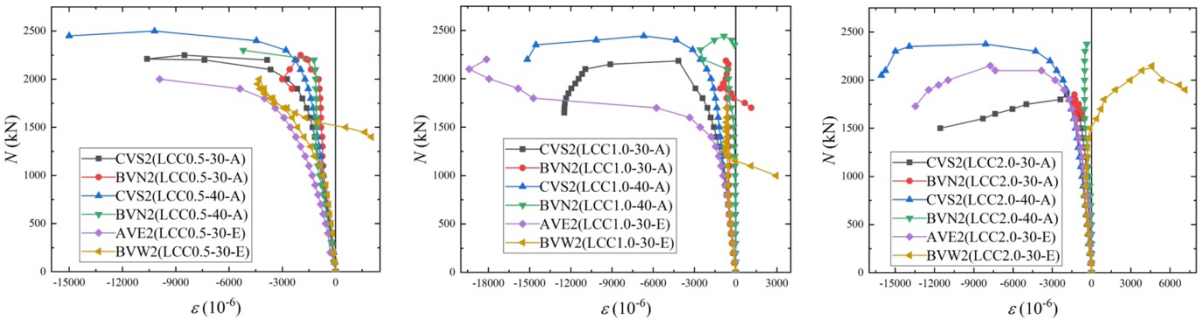

(a) 0.5 m-long specimen (b) 1.0 m-long specimen (c) 2.0 m-long specimen

Fig. 9. Load–strain curves

5. Conclusion

In order to further simplify the construction steps and expand the application scope of special-shaped concrete-filled steel tubular columns, a novel LCFSTC was proposed in this study. An experimental test was developed to verify the reliability of the LCFSTC and study its mechanical properties. The following conclusions could be drawn:

(1) No weld damage is detected in any of the LCFSTCs, indicating good structural integrity of the LCFSTCs, and all the specimens exhibited good mechanical performance. The axial-loaded specimens with a length of 0.5 m experience strength failure; the 1.0 and 2.0 m-long specimens exhibit bending instability failure. For the 0.5 m-long eccentric-loaded specimen, a failure mode intermediate between strength failure and bending failure is observed.

(2) The ductility coefficient and bearing capacity of the axial-loaded specimens both decreases as the specimen length increases. As the specimen length increased from 0.5 m to 1.0 and 2.0 m, the bearing capacity (mean value of specimens with C30 and C40 concrete grates) decreased by 2.5% and 11.1%, respectively, and the ductility coefficient decreased by 23.0% and 47.2%, respectively. When the concrete strength grade increases from C30 to C40, the average maximum load increases by 17.1%. Both the ductility coefficient and bearing capacity of the axial-loaded specimens decrease as the specimen length increases.

(3) Eccentric loading enhances the uneven force distribution, increases the bending deformation, and hence leads to an increase in the rotation angle. The angle steel underwent a transition from compression to tension. The longer the specimen is, the greater the tensile strain of the angle steel. The tensile strains of the angle steel for specimens LCC0.5-30-E, LCC1.0-30-E, and LCC2.0-30-E reached 2024, 2936, and 7150 $\mu\varepsilon$, respectively.

(4) The mechanical performance of the 1.0 and 2.0 m-long specimens is greatly affected by eccentric loading, while the bearing capacity and deformability of the 0.5 m-long specimens are minimally impacted by eccentric loading.

No weld damage was detected in any of the LCFSTCs, indicating that the square steel tubes and angle steel demonstrated well-coordinated working performance and that

all the specimens exhibited good mechanical performance. However, the number of tests is small, with only two strength grades of concrete, C30 and C40, and the tests do not include T-shaped or cross-sectional special-shaped columns. Therefore, the obtained test data are limited, and further research is needed for the promotion and application of special-shaped columns.

Acknowledgments

This work was supported by the Hunan Natural Science Foundation (2024JJ7081), the Scientific Research Project of Education Department of Hunan Province (No.20B108), the Science and Technology Innovation Project of Yiyang City (2021133), and the Aid program for Science and Technology Innovative Research Team in Higher Educational Institutions of Hunan Province.

References

[1] L. Eguchi, K. Teranishi, A. Nakagome, H. Kishimoto, K. Shinozaki, and M. Narikawa, "Application of recycled coarse aggregate by mixture to concrete construction," *Constr. Build. Mater.*, vol. 21, pp. 1542-1551, Sept. 2007.

[2] F. Alatshan, S. A. Osman, R. Hamid, and F. Mashiri, "Stiffened concrete-filled steel tubes: A systematic review," *Thin-Walled Struct.*, vol. 148, pp. 1-18. Mar. 2020.

[3] A. L. Krishan, M. A. Astafeva, and E. P. Chemyshova, "Strength calculation of short concrete-filled steel tube columns," *Int. J. Concr. Struct. Mater*., vol. 12, pp. 1-12, May. 2018.

[4] M. Ahmed, Q. Q. Liang, V. I. Patel, and N. S. H. Muhammad, "Experimental and numerical studies of square concrete-filled double steel tubular short columns under eccentric loading," *Eng. Struct*., vol. 197, pp. 205-217, Jul. 2020.

[5] W. Zhang, Z. H. Chen, and Q. Q. Xiong, "Performance of L-shaped columns comprising concrete-filled steel tubes under axial compression," *J. Constr. Steel Res.*, vol. 145, pp. 573-590, March. 2020.

[6] G. Giakoumelis and D. Lam, "Axial capacity of circular concrete-filled tube columns," *J. Constr. Steel Res*., vol. 60, pp. 1049-1068, Sept. 2004.

[7] P. Rozylo, "Stability and failure of compressed thin-walled composite columns using experimental tests and advanced numerical damage models," *Int. J. Numer. Methods Eng.*, vol. 122, pp. 5076-5099, Jun. 2021.

[8] A. Bahrami, W. H. W. Badaruzzaman, and S. Osman, "Behavior of stiffened concrete-filled steel composite (CFSC) stub columns," Lat. *Am. J. Solids Struct.*, vol. 10, pp. 409-440, Feb. 2013.

[9] K. B. Manikandan and C. Umarani, "Parametric study of CFST columns by numerical mock-up," *Mater. Today Proc.*, vol. 45, pp. 6021-6027, Nov. 2021.

[10] S. Tokgoz and C. Dundar, "Tests of eccentrically loaded L-shaped section steel fiber high strength reinforced concrete and composite columns," *Eng. Struct.*, vol. 38, pp. 134-141, May. 2012.

[11] Z. P. Chen, N. Wang, M. Zhong, J. Y. Xue, and Y. S. Su, "Experimental study and finite element analysis on normal section bearing capacity of steel reinforced concrete special-shaped columns," *J. Build. Struct*., vol. 34, no. 10, pp. 108-119. Oct. 2013. (in Chinese)

[12] Y. X. Yan, L. H. Xu, M. Yu, B. Li, and X. X. Zha, "Study of unified calculation method for eccentric-loaded capacity of special-shaped concrete filled steel tubular columns," *J. Hunan Univ.* (*Natural Sciences*), vol. 45, no. 3, pp.18-28. Mar. 2018. (in Chinese)

[13] W. H. Liu, X. Wang, Y. L. Guo, Z. H. Tian, and J. Y. Li, "Experimental and numerical study of L-shaped irregularly concrete-filled steel tube columns under axial compression and eccentric compression," *J. Build. Eng.*, vol. 84, pp. 1-21. Jan. 2024.

[14] Z. Wang, Z. Liu, and X. J. Zhou, "Experimental investigation of special-shaped concrete-filled square steel tube composite columns with steel hoops under axial loads," *Mater.*, vol. 15, no. 4179, pp. 1-23, Jun. 2022.

[15] B. Grzeszykowski and E. D. Szmigiera, "Experimental investigation on the vertical ductility of rectangular CFST columns loaded axially," *Mater.*, vol. 15, no. 2231, pp. 1-26, Mar. 2022.

[16] T. F. Ma, Z. H. Chen, Y. S. Du, T. Zhou, and Y. T. Zhang, "Mechanical properties of L-shaped column composed of RAC-filled steel tubes under eccentric compression," *Mater.*, vol. 12, no. 953, pp. 1-20, May. 2022.

[17] C. Hu, R. Cheng, Y. H. Wang, and J. C. Liu, "Design of multi-cell T-shaped concrete-filled steel tubular columns under compression and bending," *J. Constr. Steel Res.*, vol. 206, pp. 1-21. Apr. 2023.

[18] Y. L. Yang, Y. Y. Wang, F. Fu, and J. C. Liu, "Static behavior of T-shaped concrete-filled steel tubular columns subjected to concentric and eccentric compressive loads," *Thin-Walled Struct.*, vol. 95, pp. 374-388, Aug. 2015.